Romanian Reports in Physics, Vol. 64, No. 2, P. 426–435, 2012

IMAGE SURFACES STATES IN COPPER CALCULATED WITH FOURIER GRID HAMILTONIAN METHOD

D. BEJAN

University of Bucharest, Faculty of Physics, Department of Optics, P.O. Box MG 11, Bucharest, Romania
E-mail: doinitabejan@yahoo.com

Received October 20, 2010

Abstract. We used a realistic one-electron potential by Chulkov, Silkin and Echenique [1] together with the Fourier grid Hamiltonian method, developed by Clay Marston and Balint Kurti [2], to calculate the image surfaces states for Cu(100) and Cu(111) surfaces. We obtained very accurately the first 12 (15) of these for the studied surfaces.

Key words: image surfaces states, Cu(100), Cu(111), discrete variable representation (DVR), 2PPE.

1. INTRODUCTION

The image surfaces states arise through the trapping of the electron in front of a metal surface by its own image. These states are bound states with energies inside a gap of the band structure lying very close to the vacuum level and localized mostly outside the metal surface. They form a hydrogen-like Rydberg series of energy, in analogy to atomic physics.

Following the crude model of Cole and Cohen [3], the image states are bound solutions of the Schrödinger equation:

$$-\frac{\hbar^2}{2m}\nabla^2\psi\left(\vec{r}\right)+V\psi\left(\vec{r}\right)=E\psi\left(\vec{r}\right) \tag{1}$$

for an electron moving in the image potential:

$$V(z)=\begin{cases}\infty & z<0, \quad \text{in the metal}\\ -\dfrac{e^2}{16\pi\varepsilon_0 z} & z>0, \quad \text{outside the metal}\end{cases}. \tag{2}$$

For simplicity we consider that wave function of the image states should vanish for $z < 0$, *i.e.* the metal is taken to be infinitely repulsive. This is an usual way to represent the effect of the surface – that confine the electrons to a given volume – by impenetrable potential barriers.

The energy of an electron that is trapped in an image state n (n = 1,2,…) and moves parallel to the surface with the momentum $\hbar k_{\|}$ is

$$E_{n,k_{\|}} = E_n + \frac{\hbar^2 k_{\|}^2}{2m} = -\frac{me^4}{128\varepsilon_0^2 h^2 n^2} + \frac{\hbar^2 k_{\|}^2}{2m}. \tag{3}$$

The corresponding one-electron wave functions are derived from the s wave function of the hydrogen atom:

$$\psi_{n,k_{\|}}\left(z, r_{\|}\right) = N \exp(\mathrm{i}k_{\|} r_{\|})\varphi_n\left(z\right) = N \exp(\mathrm{i}k_{\|} r_{\|}) z R_{ns}\left(-\frac{z}{16\pi\varepsilon_0 a_0}\right), \tag{4}$$

where z is the distance of the electron from the surface, a_0 is the Bohr radius and N a normalization factor.

The values of the energy determined experimentally showed that actually E_n is approximately

$$E_n = -\frac{me^4}{128\varepsilon_0^2 h^2 \left(n+a\right)^2} = -\frac{0.85\mathrm{eV}}{\left(n+a\right)^2}, \tag{5}$$

where $a \leq 0.5$ is a quantum defect. Also, the E_n levels are nonstationary due to electron-electron scattering processes. Therefore, while are normally unoccupied, when populated by a laser pulse the image states decay on a finite time scale due to inelastic scattering. The lifetime τ_n of the image states was theoretically calculated by Echenique *et al.* [4] and predicted to increase like $\tau_n \approx n^3$.

Being normally unoccupied, the image surface states where first detected and identified experimentally by inverse photoemission spectroscopy and more recently by energy-resolved two-photon photoemission (2PPE) spectroscopy. Time resolved 2PPE spectroscopy (TR-2PPE) was successful exciting and probing higher lying (n = 4÷6) image states for Cu(100) [5] and other clean low-index surfaces [6, 7].

The time resolution in 2PPE provides a direct measure for lifetime effects. This lifetime can be increased by adsorbing successive layers of Xe or other rare gas, leading to decoupling of the image states from the bulk states [6, 8], but it is not influenced by metallic adatoms like Co that cause mainly quasielastic scattering of electrons in image-potential states [9]. The lifetime is correlated to the penetration p_n of the image state into the bulk [10]:

$$\tau_n = \frac{\hbar}{b\left(E_n - E_F\right) p_n}, \tag{6}$$

where E_F is the Fermi energy, b a system dependent factor and

$$p_n = \int_{bulk} \left|\varphi_n\left(z\right)\right|^2 \mathrm{d}z\,. \tag{7}$$

In eqn.(7), $\varphi_n\left(z\right)$ is the z-dependent part of the image state wave function that in general replaces the approximate expression given in eqn.(4), deduced in an ideal H-like model.

In this paper, we calculate the energies and the wave functions for the image states of Cu(100) and Cu(111) surfaces, using a one-dimensional model *i.e.* assuming the separability of the z and $r_{\|}$ motions of the active electron. For the z part, we solved the Schrödinger equation for the motion of the electron in the local, effective, one-dimensional potential of Chulkov, Silkin and Echenique [1] using the Fourier grid Hamiltonian (FGH) method of Clay Marston and Balint Kurti [2]. Then, we computed the lifetimes using eqns. (6) and (7) and we compared them with the experimental data.

The FGH method is derived from the discrete Fourier transform algorithm. The FGH is a special case of the discrete variable representation (abbreviated as DVR) methods [11, 12], having the advantage of simplicity. The FGH method requires the evaluation of the potential only at certain grid points and forward and reverse fast Fourier transforms which reduce to a summation over cosine functions. The Hamiltonian matrix elements are $H_{ij} = \frac{2}{N}\sum_{l=1}^{n} \cos\left(\frac{2\pi l\left(i-j\right)}{N}\right) T_l + V\left(x_i\right)\delta_{ij}$, where $T_l = \frac{2}{m}\left(\frac{\hbar 2\pi l}{N\Delta x}\right)^2$ and $T_0 = 0$. In particular, the eigenfunctions of the Hamiltonian operator are generated directly as the amplitudes of the wave functions on the grid points and they are not given as a linear combination of any set of basis function.

2. MODEL AND POTENTIAL

Cu(100) is one of the most studied of metal surfaces. Numerous measurements and calculations have been performed for this surface. The binding energies for n = 1,2 [13, 14] and the lifetimes for n = 1,2,…,6 [5, 7] were accurately determined experimentally. Cu(100) is one of the best candidate to model and verify the characteristics of the image surface states.

The Cu(111) surface presents another kind of image states. On this surface the energy gap is located below the vacuum level and only the first image state has the energy in the gap. All other image states are above the gap and degenerate with the bulk states. Also 2PPE [6] give a lifetime 17±5 fs for the second image state that is a lower than the lifetime 18±5 fs of the first image state, owing to the resonance character of the second image state.

For both copper surfaces we used a one dimensional model. The electron is allowed to move only along z (normal to the surface), *i.e.* we restrict to electronic states with $k_{\|} = 0$ and the obtained values of energy correspond to E_n. The Schrödinger equation for the electron is:

$$-\frac{\hbar^2}{2m}\frac{\mathrm{d}^2\varphi_n}{\mathrm{d}z^2} + V(z)\varphi_n = E_n\varphi_n, \tag{8}$$

where $V(z)$ is the local, effective potential of Chulkov, Silkin and Echenique [1]. This potential has the analytical form:

$$V(z) = V_1(z) + V_2(z) + V_3(z) + V_4(z), \tag{9}$$

where

$$V_1(z) = A_{10} + A_1 \cos\left(\frac{2\pi}{a_s} z\right), \qquad z < 0, \tag{10}$$

$$V_2(z) = -A_{20} + A_2 \cos(\beta z), \qquad 0 < z < z_1, \tag{11}$$

$$V_3(z) = A_3 \exp\left[-\alpha(z - z_1)\right], \qquad z_1 < z < z_{im}, \tag{12}$$

$$V_4(z) = \frac{\exp\left[-\lambda(z - z_{im})\right] - 1}{4(z - z_{im})}, \qquad z_{im} < z. \tag{13}$$

From the ten parameters of the potential only four parameters A_{10}, A_1, A_2, β are independent; the remaining ones are determined by forcing the potential and its first derivative to be continuous. The parameters A_1 and A_{10} reproduce the width and the position of the energy gap respectively. The solid-vacuum interface region is represented by the equations (11) and (12). The parameters A_2 and β of eqn. (11) reproduce experimental or first principles calculation values for E_0 (the surface state) and E_1 (the first image state) at $\bar{\Gamma}$ point. The intermediate point z_1, determined relative to the surface atomic layer, is given by $z_1 = 5\pi/4\beta$. The position of the image plane z_{im}, defined as the center of mass of the induced positive charge, is automatically obtained from the potential eqns. (10–13). All the parameters are given in Table 1 for both copper surfaces.

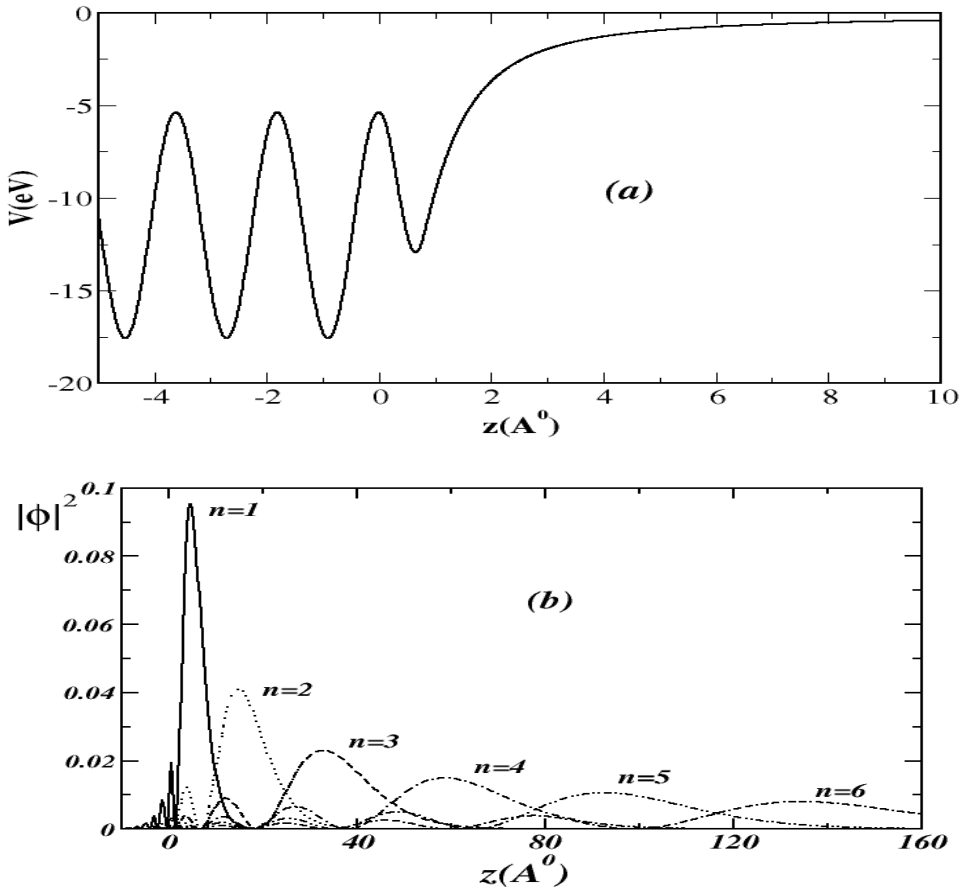

Fig. 1 – The Chulkov potential (a) and the calculated probability amplitude of the first 6 image states (b) for Cu(100).

The potential (9) is represented in Fig. 1. One can see that within the bulk region ($z < 0$), $V(z)$ is lattice periodic. At the solid-vacuum interface the potential goes over into a screened Coulomb potential. At very large distances from the surface, the screened potential becomes unscreened as described in eqn. (1).

Table 1

Potential parameters for Cu(100) and Cu(111)

Parameter	Cu(100)	Cu(111)	Parameter	Cu(100)	Cu(111)
A_{10}	–11.480	–11.895	a_s	3.415	3.94
A_1	6.10	5.14	λ=2α	2.168	2.405
A_2	3.782	4.327	z_{im}	1.202	1.114
A_{20}	–9.252	–11.082	β	2.539	2.9416

3. RESULTS

A) Cu(100). The spatial z-grid had 4096 points, spaced by an interval Δz =0.3 A°. The grid started at –614.4 A° in the bulk. We calculated the eigenstates in an energy region between –11.88 eV and about 3 eV relative to the vacuum energy E_{vac}= 0. The first 341 states are bulk electronic states, followed by the image surface states located in the projected band gap of Cu(100) that begin at –3.12, as shown in Fig. 2a. The first image state is located at – 0.57 eV in excellent agreement with the experiment [14] and is seen a bit separated in Fig. 2a.

The eigenenergies E_n of the twelve image states scale according to the ideal scaling law (5). In Fig. 2b, the quantity $\sqrt{-E_n}$ is shown as a function of n. The representative points display on a straight line. A linear fit gives a = 0.20 for the parameter from eq. (5).

In Fig. 1b we illustrated the probability amplitude for the first 6 image states calculated with the FGH method. The wave functions of the image states are located closer to the surface, in the vacuum side, but penetrate also somewhat in the bulk. For the penetration p_n we use the same limits of integration as in the paper of Klamroth, Saalfrank and Höfer [15] paper (see their eqn. 15); p_n is found to scale as:

$$p_n = \int_{-z_{im}}^{z_{im}} \left|\varphi_n(z)\right|^2 \mathrm{d}z \approx (n+a)^{-3}. \tag{14}$$

This dependence can be observed clearly in Fig. 2c, where $p_n^{-1/3}$ is shown as a function of n. A linear fit gives a = 0.22 for the parameter from eqn. (14), close to the value a = 0.20 found above for the energy representation. The calculated bulk penetration p_n can be used in the semi empirical formula (6) to estimate the lifetime τ_n where b = 0.13 [10] and E_F = – 4.62eV [15]. The energies, amount of bulk penetration and lifetimes for the first 12 image states are given in Table 2.

For the first 6 image states, experimental results are available and are also given in Table 2. Our energies and lifetimes are in good agreement with the experimental values. They also are in excellent agreement with the values obtained by Klamroth, Saalfrank and Höfer [15] using a more complicated method also based on FGH, but with a mapped Fourier grid. In their method the grid is mapped onto a non-equidistant grid by a mapping function and involves twice as many fast fourier transform (FFT) than the simple FGH method used here. The mapped Fourier grid Hamiltonian method is more accurate but also more complicated and time consuming than FGH.

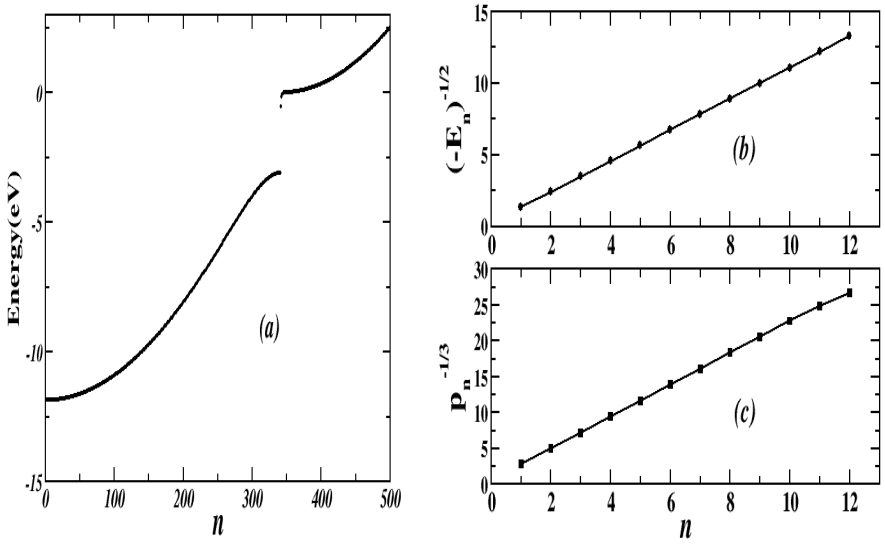

Fig. 2 – Eigenenergies (a), $\sqrt{E_n}$ (b) and $p_n^{-1/3}$ (c) for Cu(100) as function of *n*.

Table 2

n	E_n	$\sqrt{E_n}$	$p_n^{-1/3}$	Calc. $\tau_n(fs)$	$\tau_n(fs)$ **(**exp. []**)**
1	-0.573	1.320	2.745	22	40±6 [7]
2	-0.176	2.378	4.913	114	120±15 [7]
3	-0.083	3.456	7.134	344	300±20 [7]
4	-0.048	4.538	9.365	773	630 [5]
5	-0.031	5.621	11.599	1464	1200 [5]
6	-0.022	6.705	13.834	2480	2000 [5]
7	-0.016	7.789	16.068	3883	
8	-0.012	8.873	18.303	5737	
9	-0.010	9.958	20.537	8103	
10	-0.008	11.042	22.759	11027	
11	-0.006	12.152	24.824	13627	
12	-0.005	13.259	26.712	15465	

B) Cu(111). The spatial grid used for Cu(100) was also used for Cu(111). The energies are calculated from –12.27 eV and about 5 eV relative to the vacuum energy E_{vac}= 0. The first and the second image states are at – 0.82 eV and – 0.25 eV, in good agreement with 2PPE experiments [6, 16] and higher level theory [10]. However, we found the projected band gap extending from – 5.91 eV to – 0.76 eV, a bit different from the experimental observations that place it between – 5.75 eV and – 0.6 eV [6, 17]. Only the width of the gap (5.15 eV) matches well the experimental findings. We also found a surface state at – 5.31 eV (it is seen as a point in Fig. 4a) *i.e.* 0.40 eV under the Fermi level situated at – 4.91 eV. Experimentally, the surface state was found at – 0.39 eV under the Fermi level [17, 18].

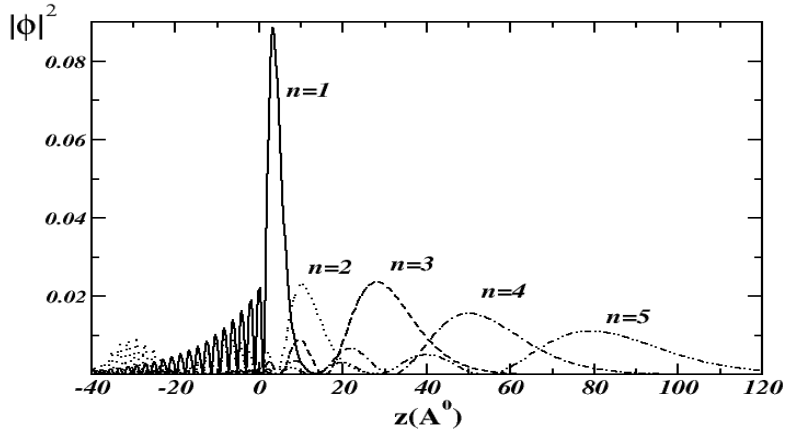

Fig. 3 – The calculated probability amplitude of the first 5 image states of Cu(111).

Another problem was to identify the real image states. The energy of the image states are intercalated with the energies of the bulk states. We separated them only observing the behavior in the bulk and in the vacuum side of the metal. The image states extend less in the bulk and more in the vacuum, the extension increasing with the quantum number as described by the approximate theoretical formula, eqn. (4). We represented the probability amplitude for the first 5 image states of Cu(111) calculated with our model, in Fig. 3. Compared with the states illustrated in Fig. 1b for Cu(100), one can see that, for Cu(111), the image states penetrate more in the bulk, achieving some bulk behavior.

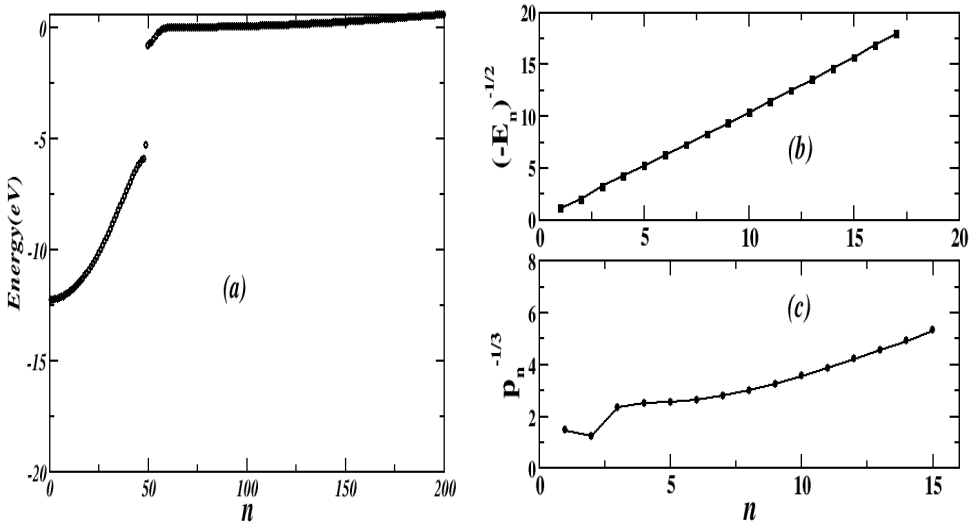

Fig. 4 – Eigenenergies (a), $\sqrt{E_n}$ (b) and $p_n^{-1/3}$ (c) for Cu(111) as function of *n*.

In Fig. 4, the quantities E_n, $\sqrt{-E_n}$, $p_n^{-1/3}$ are shown as a function of n. Their behavior is linear for $\sqrt{-E_n}$, as above for Cu(100), but nonlinear for $p_n^{-1/3}$. We found 0.32 and 0.54 for the amount of penetration p_n, for the first and the second image states, values leading to an inversion in the lifetimes of these states, in agreement with the experimental values from [6], i.e.18 ± 5 fs and 17 ± 5 fs for the first and second image state.

4. CONCLUSIONS

In this paper, we calculated the energy and wave functions for Cu(100) and Cu(111) using the FGH method [2] for solving the Schrödinger equation (8) for the electron moving in the local, effective, one-electron potential developed by Chulkov *et al.* [1]. Our FGH method is the simplest DVR method and has the great advantage that the generated wave functions are not a linear combination of any set of basis function.

For Cu(100) we found well the position of the projected energy gap and 12 image states. For the first 6 states, the values of the energies and lifetimes are in good agreement with the experimental data obtained with 2PPE [13, 14, 5, 7] and also in excellent superposition with the values calculated by Klamroth, Saalfrank and Höfer [15] using the mapped Fourier grid Hamiltonian method. For Cu(111), we also find well the position of the energy gap and the energies of the surface image states but we had to eliminate the bulk states, mixed with the image states by visualizing their bulk and vacuum behavior.

Our results demonstrate that FGH is a simple but powerful method to evaluate the eigenvalues and eigenenergies for a large class of potentials. It may be used in connection with density matrix propagation to describe the dynamics of electrons in image states [15] or adatoms desorption that involves excitation of electrons in image states [19]. We are going to use the results obtained in this paper to describe the complicated, asymmetric dynamics of electrons on image states on Cu stepped surface [20, 21].

REFERENCES

1. E. V. Chulkov, V. M. Silkin, P.M. Echenique, Surf. Sci., **437**, 330 (1999).
2. C. Clay Marston, G. G. Balint-Kurti, J. Chem. Phys., **91**, 3571 (1989).
3. M. V. Cole, M. H. Cohen, Phys. Rev. Lett., **23**, 1238 (1969).
4. P. M. Echenique, J.B. Pendry, J. Phys. C, **11**, 2065 (1978).
5. U. Höfer, I. L. Shumay, Ch. Reuβ, U. Thomann, W. Wallauer, Th. Fauster, Science, **277**, 1480 (1997).
6. M. Wolf, E. Knoesel, T. Hertel, Phys. Rev., B **54**, R5295 (1996).
7.I. L. Shumay, U. Höfer, Ch. Reuβ, U. Thomann, W. Wallauer, Th. Fauster, Phys. Rev., B **58**, 13 974 (1998).

8. W. Berthold, U. Höfer, P. Feulner, D. Menzel, Chem. Phys., **251**, 123 (2000).
9. M. Hirschmann, T. Fauster, Appl. Phys. A, **88**, 547 (2007).
10. P. M. Echenique, J. M. Pitarke, E. V. Chulkov, A. Rubio, Chem. Phys., **251**, 1 (2000).
11. J. C. Light, I. P. Hamilton, J. V. Lill, J. Chem. Phys., **82**, 1400 (1985).
12. Z. Bačič, R. M. Whitnell, D. Brown, J. C. Light, Comput. Phys. Commun., **51**, 35 (1988).
13. Th. Fauster, W, Steimann, *Electromagnetic Waves: Recent Development in Research*, Vol. 2, Elsevier, Amsterdam, 1995, p. 350.
14. K. Giesen, F. Hage, F. J. Himpsel, H. J. Riess, W. Steimann, Phys. Rev., B **35**, 971 (1987).
15. T. Klamroth, P. Saalfrank, U. Höfer, Phys. Rev., B **64**, 035420 (2001).
16. K. Giesen, F. Hage, F. J. Himpsel, H. J. Riess, W. Steimann, Phys. Rev., B **33**, 5241 (1986).
17. S. Ogawa, H. Nagano, H. Petek, A. P. Heberle, Phys. Rev. Lett., **78**, 1339 (1997).
18. W. Steimann, Appl. Phys., A **49**, 365 (1989).
19. D. Kröner, T. Klamroth, M. Nest, P. Saalfrank, Appl. Phys., A **88**, 535 (2007).
20. M. Roth, M. Weinelt, T. Fauster, P. Wahl, M.A. Schneider, L. Diekhöner, K. Kern, Appl. Phys., A **78**, 155 (2004).
21. M. Roth, T. Fauster, M. Weinelt, Appl. Phys., A **88**, 497 (2007).